Data-driven Model for the Dynamic Characteristics of O-Rings for Gas Bearing Supported Rotors

Philipp Bättig
Laboratory for Applied Mechanical Design
Department of Mechanical Engineering
Ecole Polytechnique Fédérale de Lausanne
CH-2002 Neuchâtel 2
Email: philipp.battig@epfl.ch

Jürg Schiffmann
Laboratory for Applied Mechanical Design
Department of Mechanical Engineering
Ecole Polytechnique Fédérale de Lausanne
CH-2002 Neuchâtel 2
Email: jurg.schiffmann@epfl.ch

The measurement results of various Nitrile-Butadiene-Rubber (NBR) O-Ring sizes are presented and reduced order models are developed in order to predict the stiffness and damping coefficient as a function of O-Ring geometry, Shore hardness, squeeze and excitation frequency. The results show that the curvature ratio d/D needs to be considered in the reduced order models. Assessment of the model suggests a maximum deviation of 30% in predicted stiffness compared to the measurement data. However, taking into account the typical Shore hardness tolerance given by O-Ring manufacturers and other measurement uncertainties, the proposed model enables the prediction of various O-Rings to a good accuracy in the frequency range of 1.5 to 3.75kHz which corresponds to typical gas bearing supported rotor applications.

Nomenclature

A Main effect matrix
a Main effects
A_1 Vibration amplitude housing, [m]
A_2 Vibration amplitude mass, [m]
A_{O-Ring} Vibration amplitude across O-Ring, [m]
c Viscous damping coefficient, [Ns/m]
d Cross-sectional diameter, [m]
D O-Ring diameter, [m]
D_{ext} External diameter, [m]
D_{int} Internal diameter, [m]
E^* Complex Young's modulus, [Pa]
E' Storage modulus, [Pa]
E'' Loss modulus, [Pa]
f Excitation frequency, [Hz]
k^* Complex stiffness, [N/m]
k_1 Dynamic storage stiffness, [N/m]
k_2 Loss stiffness, [N/m]
m Mass, [kg]
N Number of experiments, [-]
Sh_A Shore A hardness, [-]
X Model matrix, [-]
Y Response matrix, [-]

α Amplitude ratio $\frac{A_2}{A_1}$, [-]
δ Squeeze, [-]
ε Stretch, [-]
$\Delta\varphi$ Phase angle difference, [rad]
η Loss factor, [-]
μ Poisson ratio, [-]
ω Angular frequency, [rad/s]

1 Introduction

Gas lubricated bearings generally require very small clearances to allow stable rotor operation [1]. The consequences are high manufacturing costs, stringent misalignment tolerances and increased specific windage losses. Increased clearances are possible if the loss in rotordynamic performance is compensated by the addition of external damping [2]. External damping requires a flexible bushing support and can be introduced either through squeeze film

dampers [3, 4] or by other soft supports [5]. A commonly used procedure to stabilize gas lubricated bearings is to add external damping by supporting the bushings in a flexible manner, on O-Rings as an example [2, 6]. Figure 1 presents the evolution of synchronous motion amplitudes of O-Ring supported bearing bushings obtained from a gas bearing supported rotor accelerating from 20krpm to 220krpm, tested in our laboratory. The measurements suggest motion amplitudes peaking at 1μm.

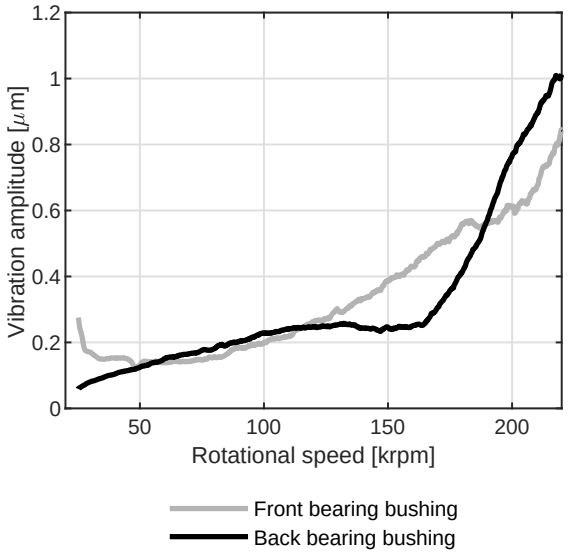

Fig. 1. Measurement of O-Ring supported bearing bushing amplitudes

The level of stiffness and damping of the flexible bearing bushing support determines the rotordynamic stability and/or the potential gain in bearing clearance. A reduced order model to predict the dynamic characteristics of O-Rings is therefore of great importance to assess and predict the rotordynamic performance of the rotor-bearing system.

The dynamic characteristics of O-Rings have been investigated by Smalley et al. [7], Tomioka et al. [8], Green et al. [9] and lately by Al-Bender et al. [10]. Most of these investigations have been performed focusing on the effects of excitation frequency, temperature, O-Ring diameter, cross-sectional diameter and squeeze on the stiffness and damping properties of various O-Ring materials. However, no reduced order model has been developed using the measurement data. Green and English [11] performed a finite element analysis of elastomeric O-Rings in axial and radial compression and present a correlation for a non-dimensional stiffness as a function of the squeeze δ. The influence of O-Ring curvature ratio d/D has been discarded after analyzing its effect by varying d/D. Al-Bender et al. [10] have performed measurements of Viton and Kalrez O-Rings and provide expressions for the frequency dependence of stiffness and damping for specific O-Ring geometries in a frequency range of 0.1-0.8kHz. Unfortunately, this range only covers the lower end of typical gas bearing supported rotors, which often rotate at speeds above 2kHz [6, 12]. Shoyama and Fujimoto [13] measured the stiffness and damping coefficients of three different NBR O-Ring diameters of constant cross-sectional diameter in the frequency range of 0.4-0.7kHz and developed a material model that can be used in FEM analysis to predict the dynamic characteristics of NBR O-Rings. Unfortunately, a simple parametric model that is not depending on FEM analysis and that is able to predict the dynamic stiffness and damping characteristics of O-Rings as a function of their geometry, squeeze, frequency and Shore hardness is still missing in the current literature.

1.1 Objectives

The goal of the investigation is a parametric model to accurately predict dynamic stiffness and damping properties of O-Rings in cyclic radial compression. The objective is to first measure the dynamic characteristics of various O-Ring sizes and to identify the major factors affecting stiffness and damping. In a second part, the objective is a data-driven reduced order model for stiffness and damping that allows the prediction of the dynamic characteristics of O-Rings as a function of their geometry and operating conditions.

1.2 Scope of the paper

In order to make the design of gas bearing supported rotors with bushings flexibly supported on O-Rings more reliable, the dynamic characteristics of 60 representative O-Rings are measured under cyclic radial loading. The results are then condensed into a reduced order model that enables the prediction of the stiffness and damping coefficients. The dynamic behavior of O-Rings is dependent on the pre-load (namely squeeze and stretch), the excitation frequency and amplitude, the dimensions, the operating temperature and the manufacturing tolerances [7].

The nomenclature of all relevant O-Ring dimensions is presented in Fig. 2 with the definition of squeeze δ and stretch ε in Eqn. (1) and Eqn. (2). It is noted that the tested O-Rings are installed in an axially unconstrained setup.

$$Squeeze\ \delta = \frac{d - \frac{1}{2}(D_{ext} - D_{int})}{d} \tag{1}$$

$$Stretch\ \varepsilon = \frac{D_{int} - D}{D} \tag{2}$$

The O-Ring material tested in this publication is Nitrile-Butadiene-Rubber (NBR) with a Shore A hardness of 70 and 90. The investigated O-Ring dimensions and squeeze δ levels are summarized in Tab. 1. According to Smalley et al. [7], the stretch ε does not have a significant effect on stiffness and damping, hence it was held constant during all experiments.

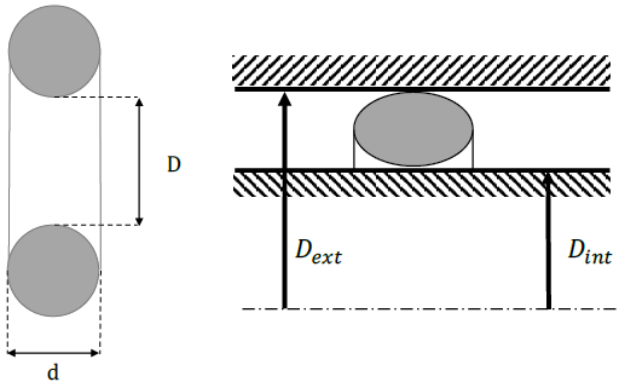

Fig. 2. O-Ring nomenclature

Table 1. Investigated O-Ring dimensions and installations

Material	NBR
Shore A hardness	70/90
Diameter D	9/14/20mm
Cross-sect. diam. d	1/2/3mm
Squeeze δ	5/10/20%
Stretch ε	1.43%

2 Experimental methodology

2.1 Measurement setup

In order to characterize the dynamic properties of O-Rings, a test rig has been designed based on the *Base Excitation - Resonant Mass Method* [7]. A schematic diagram of the modular experimental setup is presented in Fig. 3. In this test method, a non-rotating mass (1) is supported on a pair of O-Rings (2), which are held in place in a housing (3) by means of exchangeable covers (4). The housing is mounted on an electromagnetic shaker (5). The mass and O-Rings therefore form a 1-DOF damped resonant system which is excited by the vertical motion of the shaker. Measurement of the displacement of both the housing and the supported mass using capacitance displacement probes (6) enables the determination of stiffness and damping coefficients. The response of a 1-DOF system shows a natural frequency which depends predominantly on the stiffness and the supported mass. As described by Smalley et al. [7], accurate measurement data for stiffness and damping are only obtained in a frequency range where the phase angle difference between housing and supported mass lies in the range of $15-165°$. Taking this criteria into account, the natural frequency of the spring-mass oscillator has to be tuned such that it is located within the frequency range of interest. Various masses from 5.3 grams to 42.5 grams (element (1) in Fig. 3) have been designed to tune the resonance frequency within 1500-3750Hz, which is the typical range of the synchronous frequency for gas lubricated bearings. Exchangeable covers (element (4) in Fig. 3) were used to vary the O-Ring squeeze δ (5, 10 and 20%), while the stretch was held constant at $\varepsilon = 1.43\%$. The desired vibration frequency and amplitude is set using a waveform generator whose signals are fed to the shaker via an analog amplifier. The sensor signals of the capacitance displacement probes are amplified by means of a signal amplifier and then processed using LabVIEW. Table 2 summarizes the list of instruments used to perform the experiments.

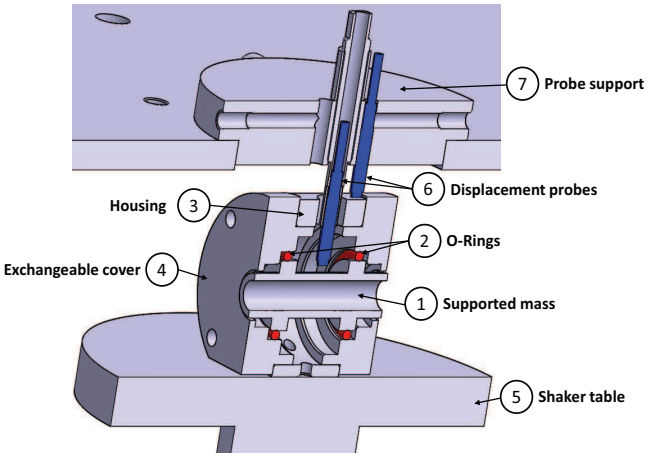

Fig. 3. O-Ring test rig

Table 2. List of instrumentation for O-Ring test rig

Device	Model
Displacement probes	Lion precision C3S
Signal amplifier	Lion Precision CPL290
DAQ system	NI PXIe-1078/6356
Electrodynamic Shaker	Labworks INC. ET-139
Analog amplifier	Labworks INC. PA-138-1
Waveform generator	Agilent 33500B-Series

2.2 Test procedure

The vibration amplitude across the O-Rings was monitored during the tests and adjusted to 0.5μm over the whole frequency range, which corresponds to typical operation of well balanced gas bearing supported high-speed rotors as presented in Fig. 1. On the O-Ring test rig, the excitation amplitude was calculated using Eqn. (3), which is valid for two sinusoidal signals of different amplitude but of identical frequency:

$$A_{O-Ring} = 2\sqrt{A_1^2 + A_2^2 - 2A_1A_2\cos(\Delta\varphi)} \qquad (3)$$

where A_{O-Ring} is the amplitude across the O-Ring, A_1 is the

Table 3. Measurement points for full factorial design

Factor	+	-
Squeeze δ	10%	5%
Shore A hardness	90	70
Diameter D	14mm	9mm
Cross-sect. diam. d	2mm	1mm
Frequency f	3000Hz	2500Hz

measured amplitude of the housing, A_2 is the amplitude of the supported mass and $\Delta\varphi$ is the phase angle difference between housing and supported mass.
The calculation of stiffness and damping for a 1-DOF model has been performed using Eqn. (4) and Eqn. (5) as presented by Gupta et al. [14]:

$$\frac{k_1}{m\omega^2} = \frac{\alpha(\alpha - \cos(\Delta\varphi))}{1 + \alpha(\alpha - 2\cos(\Delta\varphi))} \tag{4}$$

and

$$\frac{c}{m\omega} = \frac{\alpha\sin(\Delta\varphi)}{1 + \alpha(\alpha - 2\cos(\Delta\varphi))} \tag{5}$$

where k_1 is the stiffness and c is the damping coefficient of the tested O-Ring pair, m the supported mass, ω the angular excitation frequency and α the amplitude ratio of supported mass and housing A_2/A_1.
Measurements were performed in the frequency range of 1.5 to 3.75kHz for every combination of O-Ring geometry, support and material configuration, as presented in Tab. 1.

3 Measurement results

3.1 Pre-assessment of effects with a Design of Experiments (DOE) approach

In order to obtain initial insights with regards to the variables governing the stiffness and damping of O-Rings, the main relative effects have been determined using a full factorial design that allows to fit a linear model with interactions [15].
The dynamic factors investigated in this study are Shore A hardness, O-Ring diameter D, cross-sectional diameter d, squeeze δ and excitation frequency f. These five factors were varied according to Tab. 3 and the response in terms of stiffness and damping analyzed, which results in a total of $N = 2^5 = 32$ measurement points for the full-factorial experimental design. The frequency corner points for the full factorial design of NBR O-Rings were selected to be 2500 Hz and 3000 Hz whereas the squeeze δ was varied between 5% and 10%, the Shore A hardness from 70 to 90, inner diameter D from 14mm to 9mm and the cross-sectional diameter d from 2mm to 1mm. The 32x5 model matrix X is built according Hunter et al. [15] with the variables from Tab. 3 normalized from "-1" to "+1" as follows:

$$\overline{X} = -1 + 2\frac{X - X_{min}}{X_{max} - X_{min}} \tag{6}$$

This normalization enables the comparison of variables that have different metrics and orders of magnitude. The stiffness and damping coefficients can be expressed using a linear model as presented in Eqn. (7) with $a_{k_1 d}$, $a_{k_1 D}$, $a_{k_1 Sh_A}$, $a_{k_1\delta}$ and $a_{k_1 f}$ being the main effects to be investigated, here in the example of the stiffness k_1.

$$k_1 = a_{k_1 d}\cdot d + a_{k_1 D}\cdot D + a_{k_1 Sh_A}\cdot Sh_A + a_{k_1\delta}\cdot\delta + a_{k_1 f}\cdot f \tag{7}$$

Equation (7) represents a linear system of equations $Y = A\cdot X$, where A represents the matrix containing the main effects on stiffness $a_{k_1 i}$ or damping a_{ci}, Y is the response vector with the measurement results of stiffness/damping coefficients and X being the previously discussed model matrix. The main effect matrix A, containing the main effects on stiffness $a_{k_1 i}$ and damping a_{ci}, is then determined as follows:

$$A = \frac{1}{N}X^T Y \tag{8}$$

where N is the number of performed experiments. The Pareto chart of the main effects, normalized by the average measured stiffness k_1 and damping coefficient c of all $N = 32$ experiments, is presented in Fig. 4. The plot allows to identify the dominant effects on stiffness and damping. The Shore hardness is suggested to be the factor with the largest effect

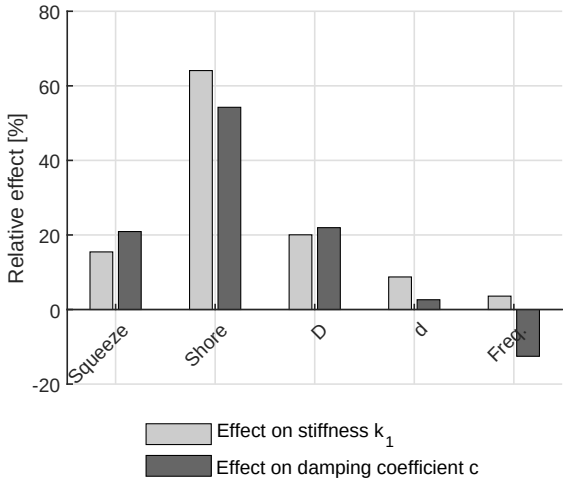

Fig. 4. Pareto chart of relative effects on stiffness and damping for the tested NBR O-Rings

on both stiffness and damping. The second most influential effect is the O-Ring diameter D, followed by the squeeze δ. The factors with the lowest effect on stiffness and damping are the cross-sectional diameter d, followed by the excitation frequency f. Note that the only factor that has a reducing effect on damping is the excitation frequency f while all other factors cause an increase in both stiffness and damping. Since all factors show non-negligible effects on the dynamic characteristics of the tested O-Rings it was decided to include all of them in the extended experimental campaign, in order to obtain a meaningful reduced order model for predicting the dynamic O-Ring properties.

3.2 Results of extended measurement campaign

Selected stiffness measurements are presented in a log-log scale as a function of frequency in Fig. 5. The results

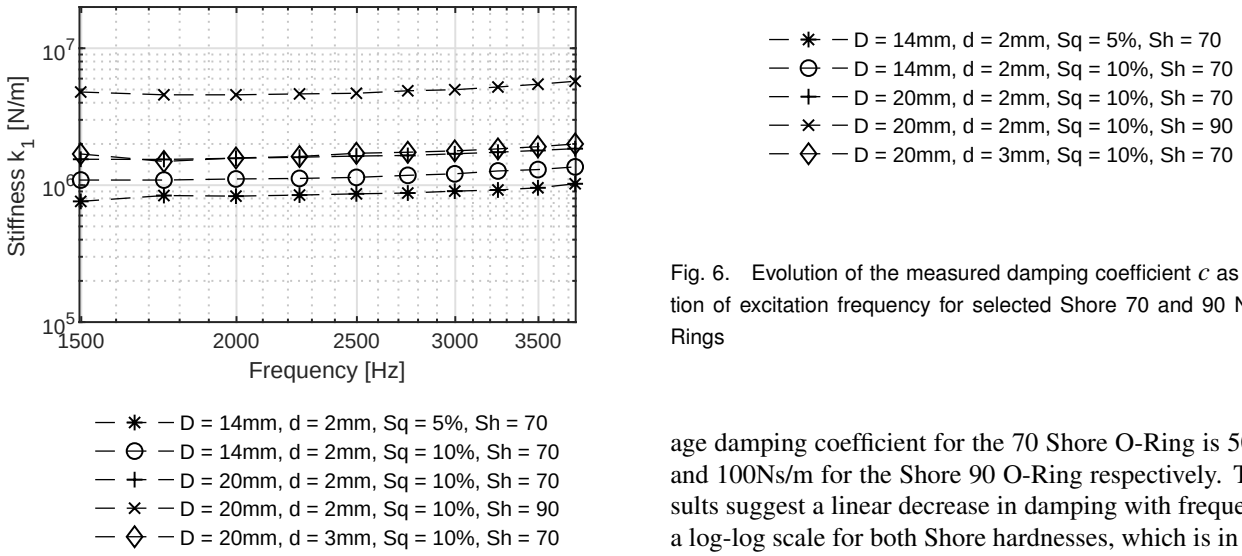

Fig. 5. Evolution of the measured stiffness k_1 as a function of excitation frequency for selected Shore 70 and 90 NBR O-Rings

suggest that the stiffness of Shore 90 O-Rings is approximately three times higher than the stiffness of the Shore 70 O-Rings within the tested frequency range. In addition, the stiffness of the investigated O-Rings seems to increase linearly with frequency in a log-log scale. This corroborates the results obtained by Smalley et al. [7], Tomioka et al. [8] and Green et al. [9]. Furthermore, the slope with which stiffness increases seems to be independent of the O-Ring diameter D, squeeze δ or the cross-sectional diameter d, which suggests that the frequency dependency is governed primarily by the material properties and is largely independent of the O-Ring geometry. General observation leads to the conclusion that the stiffness increases with increasing squeeze δ and increasing O-Ring diameter D while the cross-sectional diameter d has little effect on the stiffness and shows no clear trends. This effect has also been noticed by Green [9]. The complete set of stiffness measurement results is summarized in the appendix (Fig. 16 - 21).

Selected damping results are presented in Fig. 6. The aver-

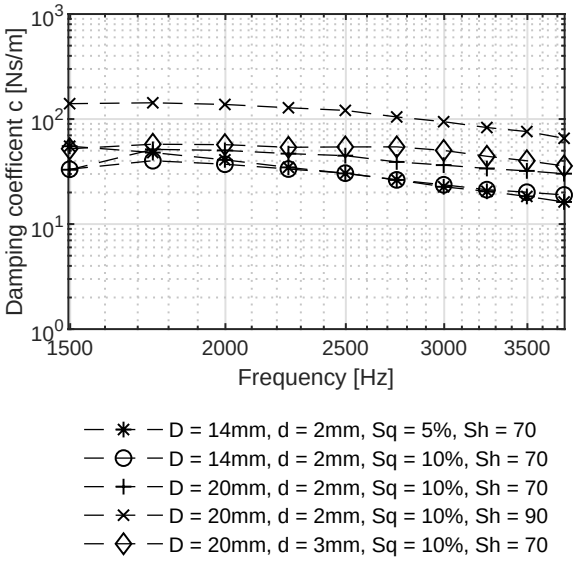

Fig. 6. Evolution of the measured damping coefficient c as a function of excitation frequency for selected Shore 70 and 90 NBR O-Rings

age damping coefficient for the 70 Shore O-Ring is 50Ns/m and 100Ns/m for the Shore 90 O-Ring respectively. The results suggest a linear decrease in damping with frequency in a log-log scale for both Shore hardnesses, which is in agreement with the previous findings from the full factorial DOE analysis. The decline in damping coefficient with increasing frequency has also been observed by Tomioka et al. [8], while the measurements of Green and Etsion [9] show an increase in damping coefficient with frequency for Buna-N but a decrease for Viton 75 O-Rings. The complete set of damping measurement results is attached in the appendix (Fig. 22 - 27).

4 Reduced order O-Ring model

4.1 Stiffness model

The objective is to obtain a dimensionless reduced order model for predicting the stiffness and damping properties of a wide spectrum of O-Rings as a function of their geometry and operating conditions, based on the experimental data. In order to condense the large amount of measured data and to enable the identification of a reduced order model for the prediction of the dynamic characteristics for different O-Rings, a dimensionless group analysis was performed. The analysis is based on the Buckingham-Pi theorem [16], which enables

the identification of the following dimensionless groups π_i:

$$\pi_0 = \frac{k_1}{E'D} \tag{9}$$

$$\pi_1 = \frac{d}{D} \tag{10}$$

$$\pi_2 = \frac{D_{int}}{D} \tag{11}$$

$$\pi_3 = \frac{D_{ext}}{D} \tag{12}$$

where E' is the storage modulus. These dimensionless groups π_i can be reorganized into the following form:

$$\pi_0 = f(\pi_1, \pi_2, \pi_3) \tag{13}$$

Combining π_1, π_2 and π_3 allows the expression of squeeze δ and stretch ε as shown in Eqns. (14) and Eqn. (15).

$$1 - \frac{1}{2}\frac{\pi_3 - \pi_2}{\pi_1} = \delta \tag{14}$$

$$\pi_2 - 1 = \varepsilon \tag{15}$$

π_1 represents the O-Ring curvature ratio d/D. Since the stretch ε was held constant in all experiments, the following relationship is obtained for the dimensionless stiffness $\underline{k}$:

$$\underline{k} = \frac{k_1}{E'D} = g(\frac{d}{D}, \delta) \tag{16}$$

In order to evaluate $\underline{k}$ based on the measured stiffness k_1, knowledge of the storage modulus E' is necessary. For the characterization of viscoelastic materials a complex modulus E^* is defined. The real part corresponds to the storage modulus E' and the imaginary one to the loss modulus E'':

$$E^* = E' + iE'' \tag{17}$$

As suggested by Kareaga [17], the storage modulus is strongly dependent on excitation frequency, temperature, vibration amplitude and other factors which leads to the conclusion that these effects can be contained in an isolated model for the storage modulus E'. Since both temperature and excitation amplitude have been kept constant throughout the experimental campaign, the storage modulus E' can be expressed by a frequency dependent component and by a second one, which is governed primarily by the Shore A hardness of the material.

Various models exist for the relationship between static storage modulus E'_0 (at $\omega = 0$) and Shore A hardness, such as proposed by Qi [18], Gent [19], Boussinesq [20], Kunz and Studer [21]. However, the model that offers the best match to the values of static storage modulus E'_0 provided by the O-Ring manufacturer is Boussinesq's, as represented in Eqn. (18)

$$E'_0 = \frac{1-\mu^2}{2RC_3} \cdot \frac{C_1 + C_2 Sh_A}{100 - Sh_A} \tag{18}$$

where μ represents the Poisson ratio and the constants $R = 0.395mm$, $C_1 = 0.549N$, $C_2 = 0.07516N$ and $C_3 = 0.025mm$, are used as presented by Kunz and Studer [21]. The frequency dependent relationship for the storage modulus E' has been obtained by averaging the frequency dependent slopes of all stiffness measurements for Shore 70 and 90 hardness. As a consequence, the combination of Boussinesq's theory for the static storage modulus E'_0 with the frequency dependence obtained from the experimental data allows to express the frequency dependent storage modulus E' as follows:

$$log(E') = a \cdot log(f) + log(E'_0) \tag{19}$$

where the coefficient a is the slope of the stiffness curves when plotted against the excitation frequency f in a log-log scale. The coefficient a was found to be $a = 0.259$ for Shore 70 and $a = 0.263$ for Shore 90 respectively. Figure 7 shows the resulting evolution of the storage modulus E' according Eqn. (19) for Shore 70 and Shore 90. The dashed lines represent the standard deviation of the averaged slope of all measured stiffness curves for Shore 70 and Shore 90 respectively. Evaluating Eqn. (16), using the frequency dependent model of E' (see Eqn. (19)), returns the dimensionless stiffness $\underline{k}$ which is frequency independent and therefore a purely geometrical function based on the dimensionless O-Ring curvature ratio d/D and the squeeze δ. As suggested by Fig. 8 for Shore 70 and by Fig. 9 for Shore 90 all the non-dimensional experimental data collapses onto a single surface. A model as in Eqn. (20), which is similar to the one used by Green, but including a linear term to account for the effect of the curvature ratio d/D, has been fitted separately to the data for Shore 70 and 90:

$$\underline{k} = a_0 + a_1 \delta^{a_2} + a_3(\frac{d}{D}) \tag{20}$$

The resulting coefficients for Shore 70 and Shore 90 NBR O-Rings to be used with Eqn. (20) are detailed in Tab. 4 as well as the coefficient of determination R^2 for both fits. The

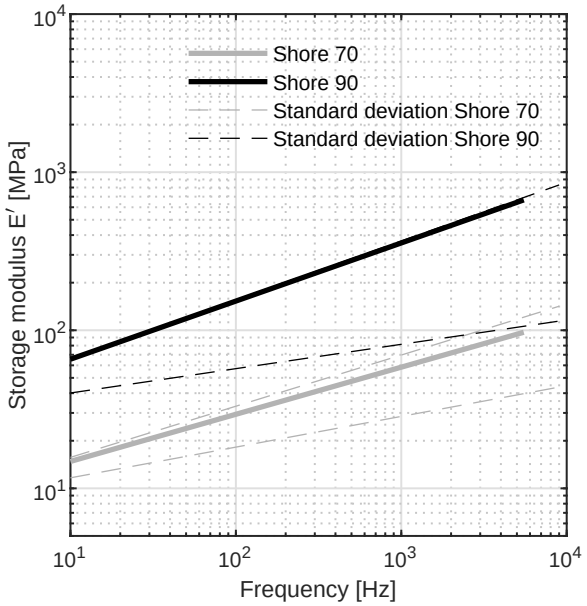

Fig. 7. Identified storage modulus E' as a function of frequency and Shore hardness

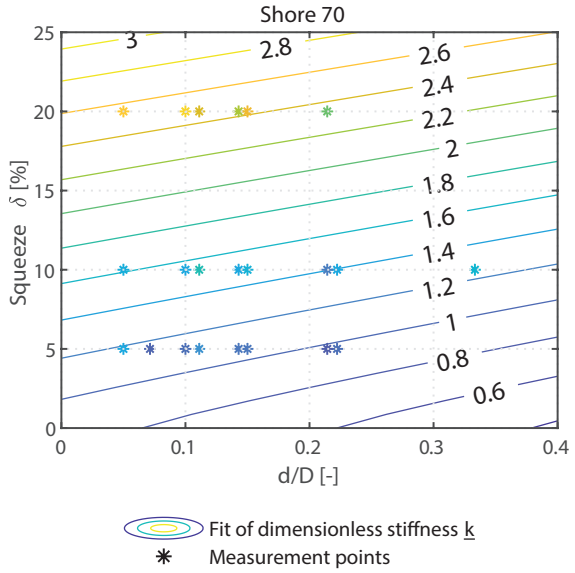

Fig. 8. Dimensionless stiffness $\underline{k}$ as a function of d/D and squeeze δ for Shore 70

Table 4. Coefficients and R^2 for dimensionless stiffness model of Shore 70 and Shore 90 NBR O-Rings

	Shore 70	**Shore 90**
a_0	0.9198	0.09614
a_1	0.0624	0.07656
a_2	1.123	1.033
a_3	-1.328	3.98
R^2	0.9143	0.8604

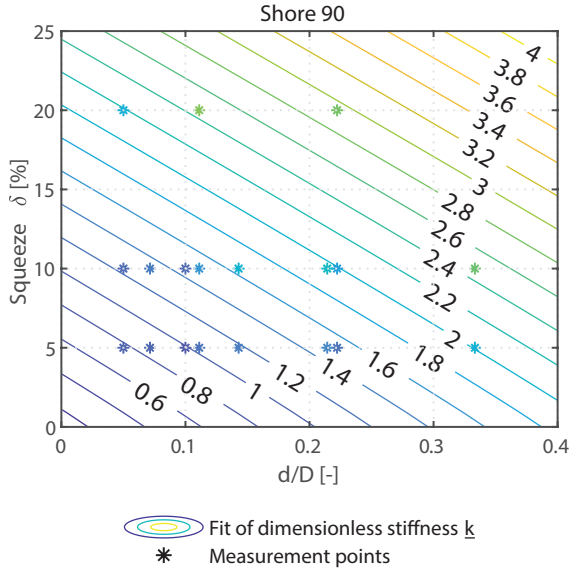

Fig. 9. Dimensionless stiffness $\underline{k}$ as a function of d/D and squeeze δ for Shore 90

dimensionless stiffness $\underline{k}$ for Shore 70 is less dependent on the curvature ratio d/D than for Shore 90 O-Rings (see Fig. 9). In addition, the comparison between the two Shore A data sets suggests an inversion of trend with regards to the effect of the curvature ratio d/D on the dimensionless stiffness $\underline{k}$. Note that Green et al. [11] suggested that the curvature ratio d/D can be neglected. They investigated the effect of the curvature ratio d/D by varying the cross-sectional diameter d, while keeping the O-Ring diameter D constant. This does not capture the real dependency of the stiffness on d/D, as presented in this paper.

4.2 Damping model

The loss factor η, commonly used to measure mechanical damping, is defined as the ratio of damping energy to strain energy [22].

$$\eta = \frac{k_2}{k_1} \tag{21}$$

where k_1 and k_2 form the complex stiffness k^* [23] of an elastomer element in the form of a mechanical impedance:

$$k^* = k_1 + ik_2 = k_1(1+i\eta) \tag{22}$$

The relationship between k_2 and the viscous damping coefficient c is defined as follows:

$$k_2 = c2\pi f \tag{23}$$

where f is the excitation frequency. Inserting Eqn. (23) into Eqn. (21) leads to a relationship between the loss factor η, k_1 and the viscous damping coefficient c, as follows:

$$\eta = \frac{c2\pi f}{k_1} \tag{24}$$

Evaluating the loss factor η for each O-Ring as defined in Eqn. (24) and averaging for Shore 70 and Shore 90 separately along the frequency f leads to the two curves for NBR O-Rings presented in Fig. 10, including the respective standard deviations for both Shore hardnesses separately. Averaging for a given Shore hardness is permitted due to the fact that the loss factor η is indicative of the visco-elastic characteristics of the measured material and is commonly used as a measure of the damping in a visco-elastic system according to the ISO 6721-1:2011 standard [24]. The results suggest that the loss factor η can therefore be assumed to be identical for all tested O-Rings of the same Shore hardness in this paper. The averaged loss factor η has been fitted by a 2^{nd} order polynomial for both Shore hardnesses:

$$\eta = a_0 + a_1 f + a_2 f^2 \tag{25}$$

with f being the excitation frequency. The averaged loss factor η for Shore 70 and Shore 90 NBR O-Rings including standard deviations and 2^{nd} order polynomial fit are presented in Fig. 10 with the coefficients summarized in Tab. 5. Knowledge of the dimensionless stiffness $\underline{k}$ and loss coefficient η therefore allows to predict the damping coefficient c using Eqn. (24) as follows:

$$c = \frac{\eta k_1}{2\pi f} = \frac{\eta \underline{k} D E'}{2\pi f} \tag{26}$$

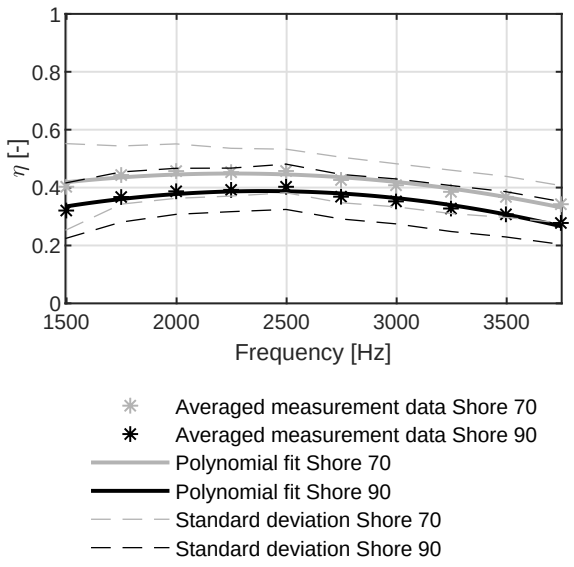

Fig. 10. Averaged loss factor η for Shore 70 and Shore 90 NBR O-Rings including standard deviations and 2nd order polynomial fit for Shore 70 and Shore 90 NBR O-Rings

Table 5. Coefficients and R^2 for 2nd order polynomial fit of loss factor η for Shore 70 and Shore 90 NBR O-Rings

	Shore 70	**Shore 90**
a_0	0.1811	0.008309
a_1	2.372e-04	3.174e-04
a_2	-5.261e-08	-6.632e-08
R^2	0.924	0.923

4.3 Reduced-order model performance and limitations

Figure 11 and Fig. 12 compare the measured and the predicted stiffness k_1 and damping coefficient c using the models presented in this paper. The dashed lines represent an error band of $\pm 30\%$. Figure 11 suggests that the error between predicted and measured stiffness is less than 30% for almost the complete data set. Only 5% of the predicted values yield errors above 30%. The prediction of the damping coefficient yields larger errors as suggested by Fig. 12, with 33% of the predicted values exhibiting an error above 30%. The differences between measurement and prediction originate from various contributions, as listed below:

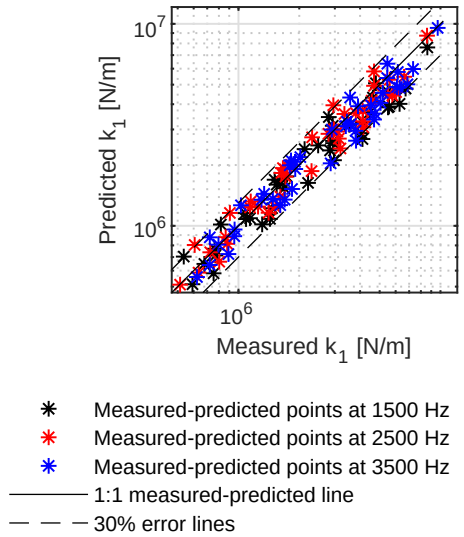

Fig. 11. Comparison of predicted and measured stiffness k_1

Measurement errors. The expected effect from measurement

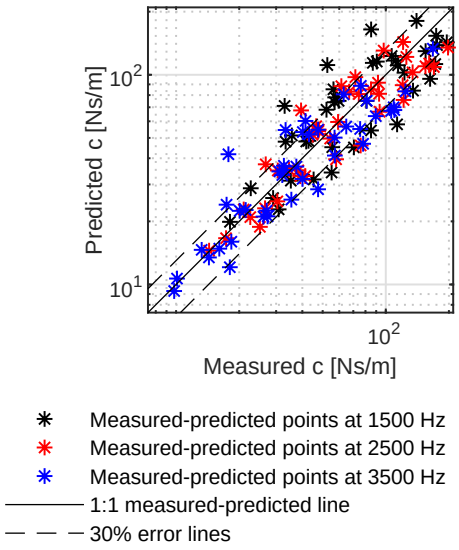

Fig. 12. Comparison of predicted and measured damping coefficient c

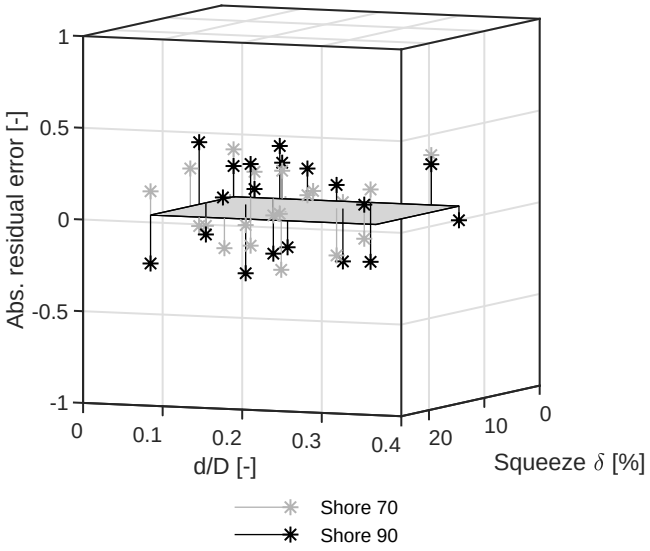

Fig. 13. Residual error of fitted surface of dimensionless stiffness vs d/D and squeeze δ

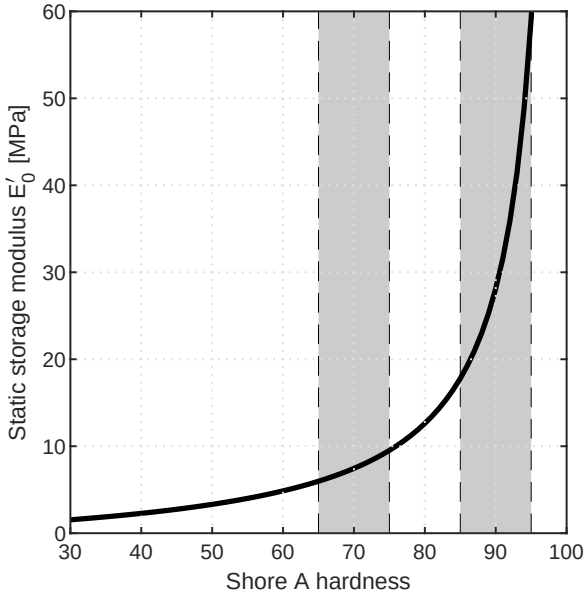

Fig. 14. Plot of static storage modulus E'_0 as a function of Shore hardness according Eqn. 18

errors of phase angle, housing and supported mass amplitudes, excitation frequency as well as the weight of the supported mass on the calculated stiffness k_1 and damping coefficient c when evaluating Eqn. (4) and Eqn. (5) were estimated using the approach of Gaussian error propagation and sum up to a maximum of $\pm 8.1\%$.

Model of storage modulus E'. The error from the proposed frequency dependent storage modulus E' model (see Fig. 7) has been analyzed by evaluating the standard deviation of the identified E' slopes that were derived from the frequency dependent stiffness measurements.

Dimensionless stiffness model. The uncertainty introduced by the reduced order model for the dimensionless stiffness $\underline{k}$ as a function of curvature ratio d/D and squeeze δ has been assessed by analyzing the fitted surface in Fig. 8 and Fig. 9. The residuals represent the differences between the measured data and the fitted surface and are plotted in Fig. 13. The largest relative residual is -34.8% which corresponds to the measured 90 Shore O-Ring of D=20mm, d=2mm (d/D = 0.1) and a squeeze δ of 10%. The measurement results suggest a dimensionless stiffness $\underline{k}$=0.9801 while the model according Eqn. (20) suggests $\underline{k}$=1.3202.

Shore hardness tolerance. The tolerance for Shore A hardness indicated by the manufacturer for the tested O-Rings in this paper is ± 5 Shore A, which is typical for mass-produced O-Rings. As previously presented in Eqn. (18), the static storage modulus E'_0 is a function of the Shore hardness and strongly affects the measured dynamic characteristics (see Eqn. (18)). In order to visualize the effect of Shore hardness deviation on the static storage modulus E'_0, Boussinesq's relation (see Eqn. (18)) is represented in Fig. 14. The gray areas represent the typical hardness tolerance of ± 5 Shore A as given by the O-Ring manufacturer. For a Shore 70 material the deviation of ± 5 Shore A yields a variation of $+28\%$ and -20% whereas for a Shore 90 material the variations are $+110\%$ and -37% respectively.

Handling inconsistencies. In agreement with the findings of Green and English [11], the experiments showed that sliding the mass into the O-Rings may introduce some uncertainty to the measurements due to twisted or nonplanarly fitted O-Rings. Measurements of O-Rings featuring a small cross-sectional diameter d suffer the most from this uncertainty since they are prone to twist during assembly. This effect has been minimized by lubricating the O-Rings that are prone to twist with demineralized water before fitting, which was then

left to evaporate before testing. The errors induced by this effect are difficult to measure.

Geometrical tolerances. Geometrical deviations of the O-Ring size compared to its specification as well as manufacturing tolerances of the test section parts can lead to further measurement errors.

In order to assess the impact of the different error components, Fig. 15 presents the measured stiffness evolution of the O-Ring with the highest residual error as discussed before (Shore 90, D=20mm, d=2mm, $\delta = 10\%$) and compares it to the prediction from the model presented in this paper. The dashed lines represent the expected measurement uncertainty while the dash-dotted lines include both measurement and Shore 90 hardness uncertainty. As suggested by

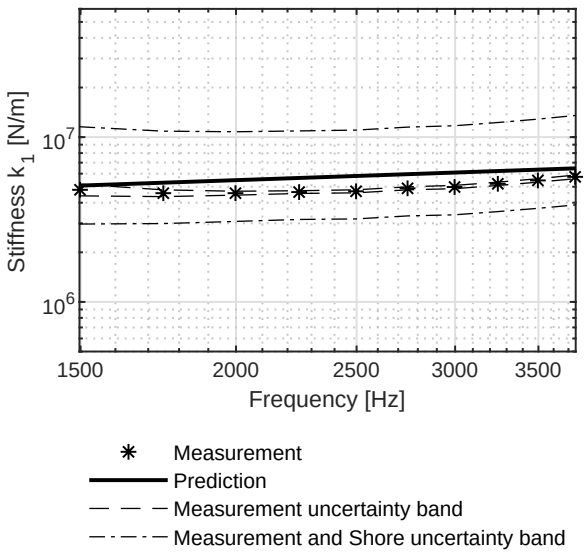

Fig. 15. Measured O-Ring stiffness compared to predicted stiffness for Shore 90, D=20mm, d=2mm, $\delta = 10\%$. Dashed lines represent measurement uncertainty while dash-dotted lines include measurement and Shore hardness uncertainty.

the dashed lines in Fig. 15 the estimated measurement uncertainty increases when moving away from the resonance frequency ($\approx 2500Hz$) of the 1-DOF system. This corroborates the recommendation by Smalley et al. [7], that measurement data should be obtained in a frequency range where the phase angle difference between housing and supported mass falls within the range of $15 - 165^\circ$. Furthermore, Fig. 15 suggests that the model proposed in this paper overestimates the stiffness of the worst case O-Ring by 35%. However, the uncertainty caused by the typical hardness tolerance of ± 5 Shore A given by the O-Ring manufacturer, which can lead to a variation in stiffness of up to 110% in the case of Shore 90 O-Rings, puts the relatively high errors of the proposed model into perspective.

5 Conclusions

In this paper a test procedure is described to determine the dynamic properties, namely stiffness and damping coefficient, of elastomeric O-Rings in cyclic radial compression. The effects of O-Ring diameter D, cross-sectional diameter d, squeeze δ, Shore A hardness and excitation frequency f have been investigated experimentally and identified as the main governing effects on the dynamic characteristics using a full factorial experimental design. Measurements of a wide range of O-Ring combinations enabled the determination of a novel non-dimensional reduced order model for O-Ring stiffness and damping based on actual measurements.

Contrary to the presented model by Green and English [11], it was found that the O-Ring cross-sectional diameter d does have an effect on the stiffness and damping coefficients of the O-Rings investigated in this paper. Further, it was found that the curvature ratio d/D does affect the stiffness and damping of Shore 70 and Shore 90 O-Rings in a different way. At a constant squeeze, increasing d/D yields a reduction in stiffness for a Shore 70 O-Ring whereas it increases stiffness for a Shore 90 O-Ring. Additional measurements with O-Rings of an intermediate Shore hardness would be needed to investigate the transition from Shore 70 to Shore 90 in more detail.

The reduced order model for stiffness and damping presented in this paper separates the geometrical O-Ring effects from the visco-elastic material properties that have an impact on the storage modulus E' and loss coefficient η, namely excitation frequency and Shore hardness as investigated in this paper. This approach allows the extension of the presented model to accommodate additional effects like temperature and excitation amplitude by including them in the models for storage modulus E' and loss factor η. Furthermore, the modular approach of the presented model allows its modification and use for various other applications, for example in tuned mass dampers or as centering springs in squeeze film dampers.

Acknowledgements

The authors acknowledge the funding by the Swiss National Science Foundation, grant PYAPP2_154278/1.

References

[1] Schiffmann, J., 2013. "Enhanced groove geometry for herringbone grooved journal bearings". *Journal of Engineering for Gas Turbines and Power,* **135**.

[2] Belforte, Colombo, Federico, Raparelli, Terenziano, and Viktorov, 2008. "High-speed rotor with air bearings mounted on flexible supports: test bench and experimental results". *Transactions of ASME: Journal of Tribology,* **130**.

[3] Szeri, A., Raimondi, A., and Giron-Duarte, A., 1983. "Linear force coefficients for squeeze-film dampers".

Transactions of ASME: Journal of Lubrication Technology, **105**.

[4] Zeidan, F. Y., Andres, L. S., and Vance, J., 1996. "Design and application of squeeze film dampers in rotating machinery". *Proceedings of the 25th Turbomachinery Symposium*, pp. 169–188.

[5] Somaya, K., Miyatake, M., Okubo, K., and Yoshimoto, S., 2015. "Threshold speed of instability of a herringbone-grooved rigid rotor with a bearing bush flexibly supported by straight spring wires". *Proceedings of ASME Turbo Expo 2015: Turbine Technical Conference and Exposition GT2015*.

[6] Waumans, T., Peirs, J., Al-Bender, F., and Reynaerts, D., 2011. "Aerodynamic journal bearing with a flexible, damped support operating at 7.2 million dn". *Journal of Micromechanics and Microengineering*.

[7] Smalley, A., Darlow, M., and Mehta, R., 1978. "The dynamic characteristics of o-rings". *Transactions of ASME: Journal of Mechanical Design,* **100**.

[8] Tomioka, J., and Miyanaga, N., 2008. "Measurement of dynamic properties of o-rings and stability threshold of flexibly supported herringbone grooved aerodynamic journal bearings". *Tribology Online,* **3**.

[9] Green, I., and Etsion, I., 1986. "Pressure and squeeze effects on the dynamic characteristics of elastomer o-rings under small reciprocating motion". *Transactions of ASME: Journal of Tribology,* **108**.

[10] Al-Bender, F., and Colombo, F., 2017. "Dynamic characterization of rubber o-rings: Squeeze and size effects". *Hindawii: Advances in Tribology*.

[11] Green, I., and English, C., 1992. "Analysis of elastomeric o-ring seals in compression using the finite element method". *Tribology Transactions,* **35**.

[12] Javed, A., Arpagaus, C., Bertsch, S., and Schiffmann, J., 2016. "Small-scale turbocompressors for wide-range operation with large tip-clearances for a two-stage heat pump concept". *International Journal of Refrigeration*.

[13] Shoyama, T., and Fujimoto, K., 2018. "Calculation of high-frequency dynamic properties of squeezed o-ring for bearing support". *Mechanical Engineering Journal,* **5**.

[14] Gupta, P., Tessarzik, J., and Cziglenyi, L., 1974. Development of procedures for calculating stiffness and damping properties of elastomers in engineering applications - part ii: Elastomer characteristics at constant temperature. Tech. rep., Mechanical Technology Incorporated.

[15] Box, G. E. P., Hunter, W. G., and Hunter, J. S., 2005. *Statistics for Experimenters - Design, Innovation, and Discovery, 2nd Edition*. Wiley series in Probability and Statistics. J. Wiley & Sons.

[16] Yarin, L., 2012. *The Pi-Theorem*. Experimental Fluid Mechanics. Springer-Verlag Berlin.

[17] Kareaga, Z., 2016. "Dynamic stiffness and damping prediction on rubber material parts, fea and experimental correlation". PhD thesis, London Metropolitan University.

[18] Qi, H. J., Joyce, K., and Boyce, M. C., 2003. "Durometer hardness and the stress-strain behavior of elastomeric materials". *Rubber Chemistry and Technology,* **76**(2), pp. 419–435.

[19] Gent, A., 1958. "On the relation between indentation hardness and young's modulus". *Rubber Chemistry and Technology,* **31**, pp. 896–906.

[20] Boussinesq, J., 1885. *Application des potentiels à l'étude de l'équilibre et du mouvement des solides élastiques*. Gauthier-Villars.

[21] Kunz, J., and Studer, M., 2006. "Determining the modulus of elasticity in compression via the shore a hardness". *Kunststoffe international,* **06**.

[22] Carfagni, M., Lenzi, E., and Pierin, M., 1998. "The loss factor as a measure of mechanical damping". *Proceedings of SPIE - The International Society for Optical Engineering*, pp. 580–.

[23] Darlow, M., and Zorzi, E., 1981. *Mechanical Design Handbook for Elastomers*. NASA.

[24] ISO 6721-1:2011(E):, 2011. Plastics – determination of dynamic mechanical properties– part 1: General principles. Standard, International Organization for Standardization, Mai.

Appendix A: Detailed stiffness and damping measurement results

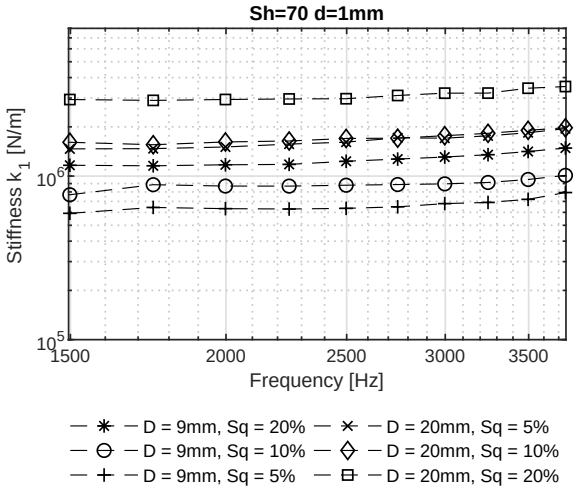

Fig. 16. Measurement results for stiffness k_1 of a Shore 70 NBR O-Ring with d=1mm

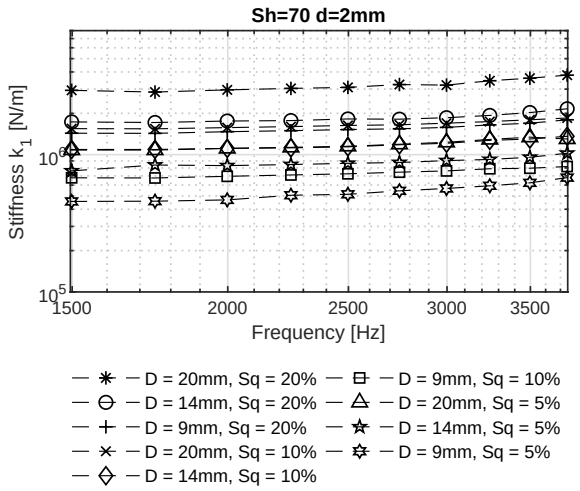

Fig. 17. Measurement results for stiffness k_1 of a Shore 70 NBR O-Ring with d=2mm

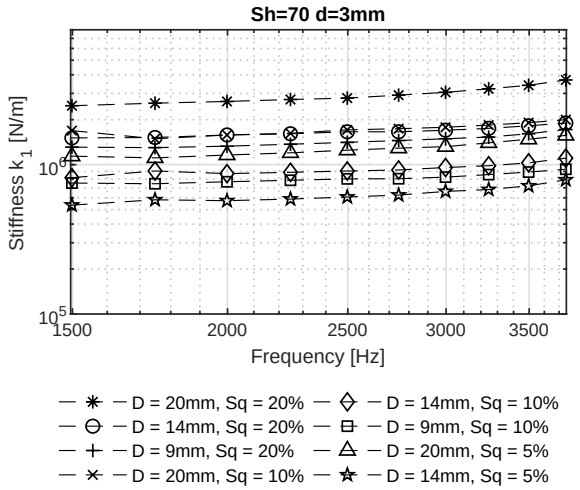

Fig. 18. Measurement results for stiffness k_1 of a Shore 70 NBR O-Ring with d=3mm

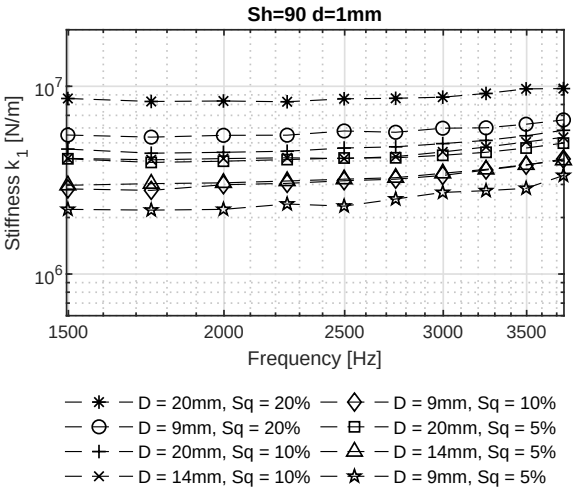

Fig. 19. Measurement results for stiffness k_1 of a Shore 90 NBR O-Ring with d=1mm

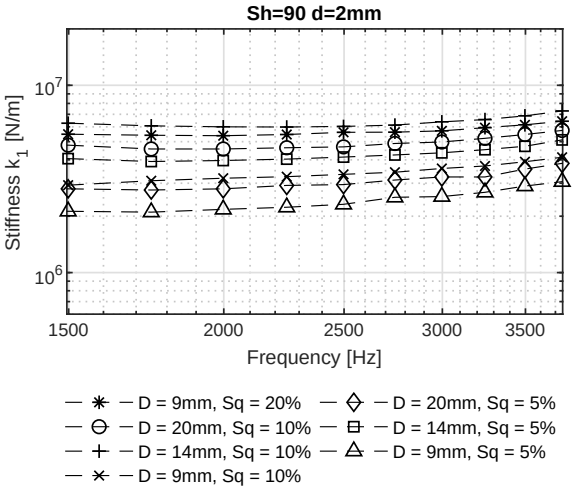

Fig. 20. Measurement results for stiffness k_1 of a Shore 90 NBR O-Ring with d=2mm

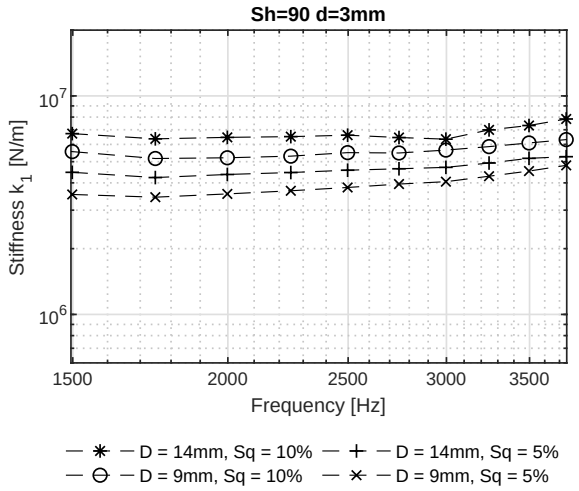

Fig. 21. Measurement results for stiffness k_1 of a Shore 90 NBR O-Ring with d=3mm

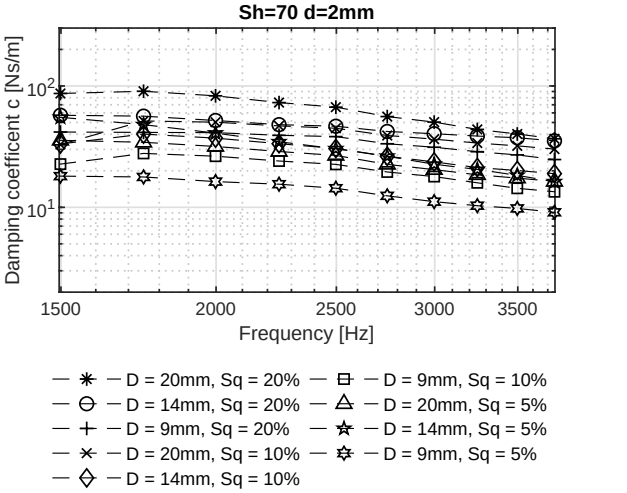

Fig. 23. Measurement results for damping coefficient c of a Shore 70 NBR O-Ring with d=2mm

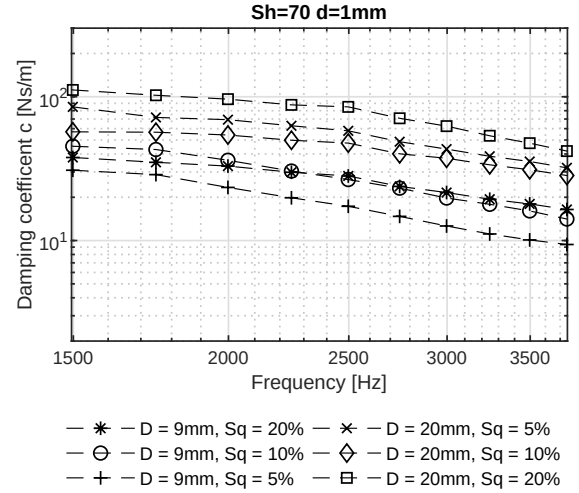

Fig. 22. Measurement results for damping coefficient c of a Shore 70 NBR O-Ring with d=1mm

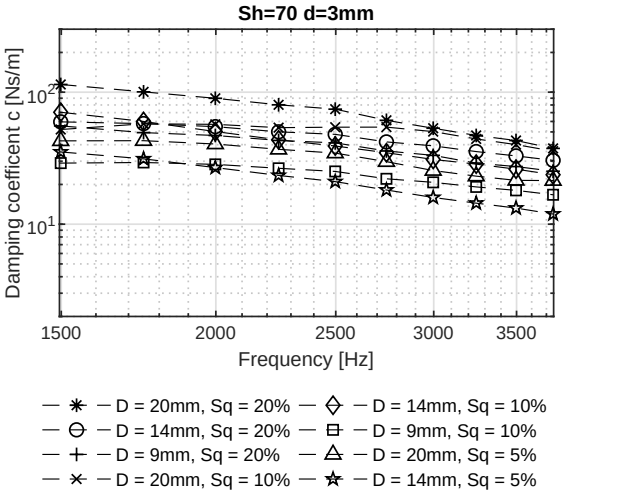

Fig. 24. Measurement results for damping coefficient c of a Shore 70 NBR O-Ring with d=3mm

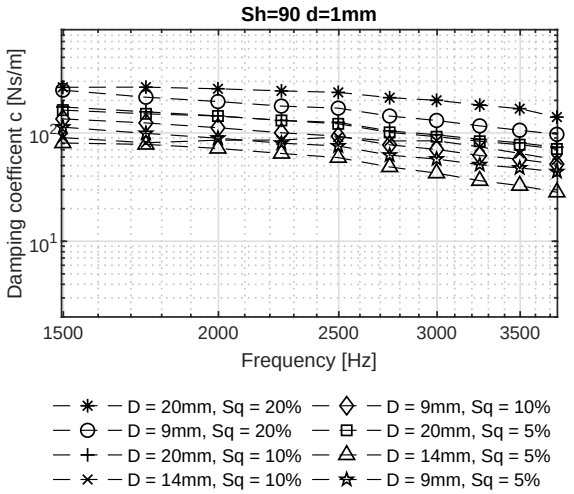

Fig. 25. Measurement results for damping coefficient c of a Shore 90 NBR O-Ring with d=1mm

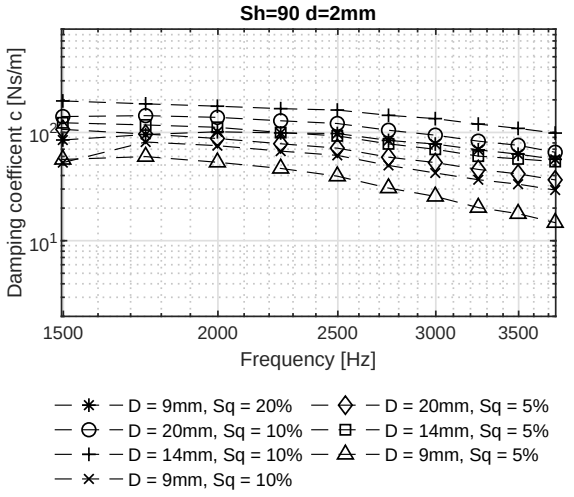

Fig. 26. Measurement results for damping coefficient c of a Shore 90 NBR O-Ring with d=2mm

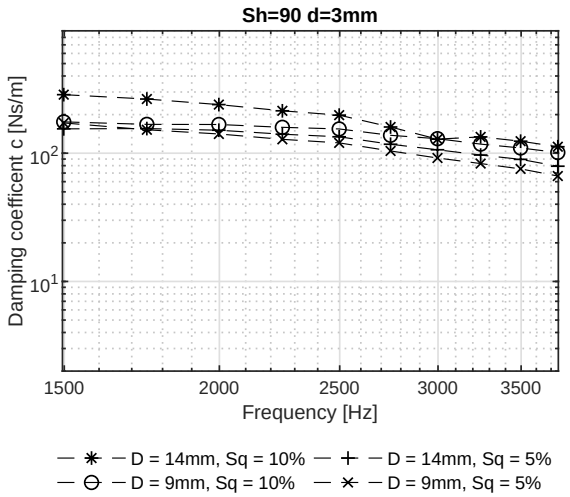

Fig. 27. Measurement results for damping coefficient c of a Shore 90 NBR O-Ring with d=3mm